Acta Crystallographica Section B
Structural Science
ISSN 0108-7681

Structure determination of structurally complex $Ag_{36}Li_{64}$ gamma-brass

Tatsuo Noritake,[a]* Masakazu Aoki,[a] Shin-ichi Towata,[a] Tsunehiro Takeuchi[b] and Uichiro Mizutani[c]

[a]Toyota Central R&D Laboratories Inc., Nagakute, Aichi 480-1192, Japan, [b]Ecotopia Science Institute, Nagoya University, Furo-cho, Chikusa-ku, Nagoya 464-8603, Japan, and [c]Toyota Physical and Chemical Research Institute, Nagakute, Aichi 480-1192, Japan

Correspondence e-mail: e0553@mosk.tytlabs.co.jp

Received 12 June 2007
Accepted 8 August 2007

The crystal structure of the $Ag_{36}Li_{64}$ gamma-brass was determined by analyzing the powder diffraction pattern taken using a synchrotron radiation beam with wavelength 0.50226 Å. It turned out that the compound contained 52 atoms in its unit cell with the space group $I\bar{4}3m$ and that the Li atom enters exclusively into inner tetrahedral (IT) and cubo-octahedral (CO) sites, whereas the Ag atom enters into those on outer tetrahedral (OT) and octahedral (OH) sites in the 26-atom cluster. Small amounts of Li also exist in OT and OH sites, resulting in chemical disorder. We discovered that the volumes of the IT and CO polyhedra shrink, while those of the OT and OH polyhedra expand relative to those of the corresponding polyhedra in the original b.c.c. (body-centered cubic) structure. This feature is universal and is found in other gamma-brasses such as Cu_5Zn_8 and Al_8V_5, for which the structure data are available. Among these gamma-brasses, we revealed the unique bond-length distribution for pairs connecting the atom on OH sites and that on CO sites, depending on the degree of *d–p* orbital hybridization between the transition metal elements such as Ag, Cu and V on OH sites, and the non-transition metal elements such as Li, Zn and Al on CO sites. It is suggested that this may hold a clue to resolving why some gamma-brasses such as the present Ag–Li and Cu–Zn possess a finite solid solution, but others such as Al_8V_5 and Mn_3In exist as line compounds.

1. Introduction

Following the first identification of the crystal structure for the Cu_5Zn_8 gamma-brass (Bradley & Thewlis, 1926), a large number of gamma-brasses possessing 52 atoms in the cubic unit cell had been discovered by the early 1930s. This includes not only systems like Cu_5Zn_8 and Cu_9Al_4, consisting of noble metals Cu, Ag and Au and polyvalent elements (Westgren & Phragmen, 1928, 1929; Bradley, 1929; Bradley & Jones, 1933), but also those involving transition metal elements *TM* = Fe, Co, Ni, Pd and others. Ekman (1931) pointed out that the Zn-TM gamma-brasses were stabilized in a range of electrons-per-atom ratios (*e*/*a*) centered at *ca* 1.6, provided that the valency of the transition metal element TM was zero. However, the presence of the gamma-brass structure was reported even in the Ag–Li alloy system (Pastorello, 1930, 1931), where the valency of both Ag and Li is apparently unity. The structure of the alloy Ag_3Li_{10} was first proposed in 1933 to possess a gamma-brass structure with a lattice constant of 9.94 Å (Perlitz, 1933).

The up-to-date phase diagram in the Ag–Li system compiled by Okamoto (2000) is based on the work by Freeth & Raynor (1953–1954). They admitted difficulty in accurately determining the phase diagram, particularly when the Li

concentration was higher than 60 at. % because of the increasing volatility and reactivity of lithium. They concluded from their microstructure, thermal arrests and X-ray diffraction studies that the gamma-brass field is divided into three slightly different phases: denoted as γ_1, γ_2 and γ_3, separated by the respective two-phase fields. The homogeneous γ_3 structure was located in the Li concentration range from 63 to 73 at.%. The diffraction patterns of γ_2 and γ_3 were very similar to each other, but careful inspection revealed characteristic differences in the intensities of the diffraction lines. Indeed, a two-phase region between γ_2 and γ_3 was revealed for the 74.46 at.% Li sample by the presence of lines arising from both structures in the X-ray diffraction pattern. Similarly, they revealed the homogeneous γ_1 structure over approximately 87 to 93 at.% Li concentration range, which was also satisfactorily indexed in terms of the gamma-brass structure.

It had already been well recognized by the late 1930s that a number of gamma-brasses are stabilized at *e*/*a* near 21/13 or 1.6, regardless of the solute concentration, and have been regarded as being typical of obeying the Hume–Rothery electron concentration rule (Witte, 1937; Mott & Jones, 1936). Mott & Jones (1936) were the first to explain the empirical Hume–Rothery electron concentration rule for gamma-brass by showing that the free-electron Fermi sphere simultaneously touches its characteristic zone planes of {330} and {411} at *e*/*a* = 1.538. More recently, the stability mechanism in a series of gamma-brasses at *e*/*a* near 21/13 or 1.6 could be successfully interpreted by analyzing the Fourier spectrum of wavefunctions derived from the first-principles FLAPW (full potential linearized augmented plane wave) band calculations (Asahi *et al.*, 2005*a*,*b*; Mizutani *et al.*, 2006). However, the Ag–Li gamma-brass consisting of only monovalent elements Ag and Li is obviously the exception to this interpretation. We consider an accurate determination of the crystal structure of the Ag–Li gamma-brass to be made as a first step in order to shed more light on the stability mechanism of the Ag–Li gamma-brass.

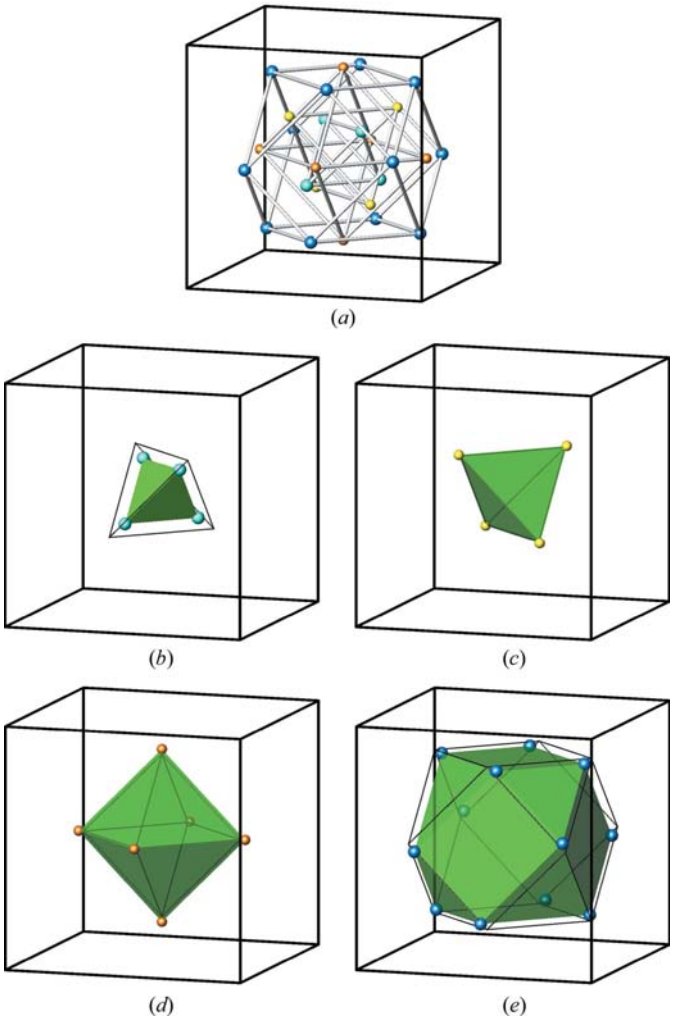

Figure 1
Structure of the 26-atom cluster consisting of the four polyhedral sites IT, OT, OH and CO sites in the $Ag_{36}Li_{64}$ gamma-brass. The corresponding polyhedra in the b.c.c. lattice are shown by thin lines. The shrinkage of the polyhedron relative to that in the b.c.c. lattice is seen in IT and CO sites, while the expansion is in OT and OH sites.

Arnberg & Westman (1972*a*,*b*) attempted to determine for the first time the crystal structure of the γ_3 phase having the composition $Ag_{30.2}Li_{69.8}$ by analyzing the diffraction pattern taken by using X-ray powder photographs with Cu $K\alpha$ radiation. They identified its structure as stacking the 26-atom cluster composed of 4, 4, 6 and 12 atoms at the vertices of the inner tetrahedral (IT), outer tetrahedral (OT), octahedral (OH) and cubo-octahedral (CO) sites, respectively, to form the b.c.c. lattice with the space group $I\bar{4}3m$. The 26-atom cluster together with the four different polyhedral sites IT, OT, OH and CO are illustrated in Fig. 1. However, the reliability factor R_I is reduced to only about 10% because of the difficulty in handling it in air. The present work is not intended to clarify any structural difference in the three gamma-brasses γ_1, γ_2 and γ_3, but to determine the crystal structure of the least volatile γ_3 phase as accurately as possible by performing the Rietveld structure analysis for the powder diffraction pattern taken by using the synchrotron radiation facility. The characteristic features of the crystal structure thus determined will be discussed in comparison with those in other gamma-brasses already studied.

2. Experimental

The alloys were prepared from silver shots of purity 99.99% and a lithium sheet of purity 99+% supplied from High Purity Materials Kojundo Chemical Laboratory Co., Ltd, Japan. According to the Ag–Li equilibrium phase diagram (Okamoto, 2000), the γ_3 phase extends from 63 to 73 at.% Li. We made the Ag–Li gamma-brass alloys at 64, 70 and 73 at.% Li. Weighed amounts of pure elements were melted in a molybdenum crucible in an induction furnace for approximately 30 s and allowed to solidify without quenching. The nominal composition was accepted, since the loss of Li during melting turned out to be negligibly small. The resulting ingot was subsequently heat-treated at 458 K for 10 d. The 64 at.% Li sample was relatively brittle and could be ground into fine powders using an agate mortar. However, two other Li-rich

samples were so soft that fine powders were hard to obtain. All the operations described above were conducted in a glove-box filled with flowing purified argon gas (dew point below 180 K).

The structural quality of the three samples was first checked using an X-ray diffractometer with Cu $K\alpha$ radiation (Rigaku, RINT-TTR). The powders were firmly mounted onto a 15 mm-square shallow hollow of the holder and its surface was fully covered with a polyimide film of 25 μm thick to protect the volatile powders from oxidation. We found that measured diffraction lines for the three samples were indexed in terms of the gamma-brass structure, but with some impurity lines, which were identified as the residual CsCl-type β-phase AgLi plus a third phase. The lattice constant of the gamma-brass was determined from the measured diffraction pattern and plotted in Fig. 2 as a function of the nominal Li concentration. It increases with increasing Li content in accordance with the difference in metallic radii (Pearson, 1972) between Ag and Li (r_{Ag} = 1.445 and r_{Li} = 1.562 Å). The degree of randomness in crystalline orientations of powders was studied by measuring the ω-scan profile centered at both the 211 and 330 + 411 reflections. The 330 + 411 reflection data for the 64 at.%Li sample is shown in Fig. 3. The smooth curve in the ω scan can be taken as evidence for the absence of any preferred orientations of grains.

Encouraged by the data above, we encapsulated 64 at.% Li fine powders into a capillary glass tube with the diameter of 0.2 mm in the glove-box mentioned above, and sealed the tube with resin to protect the sample from oxidation. The powder diffraction pattern was measured at room temperature at the BL02B2 beamline of the synchrotron radiation facility SPring-8, Japan. The incident X-ray wavelength λ was tuned to 0.50226 Å from the K-absorption edge of Ag at λ = 0.48 Å. The random orientation of grains in a capillary tube was confirmed from the uniformity in intensity of the Debye rings on the imaging plate. The Rietveld structure analysis (Izumi & Ikeda, 2000) was performed using the data over the scattering angle 2θ of 2–52°. Experimental details are listed in Table 1.[1]

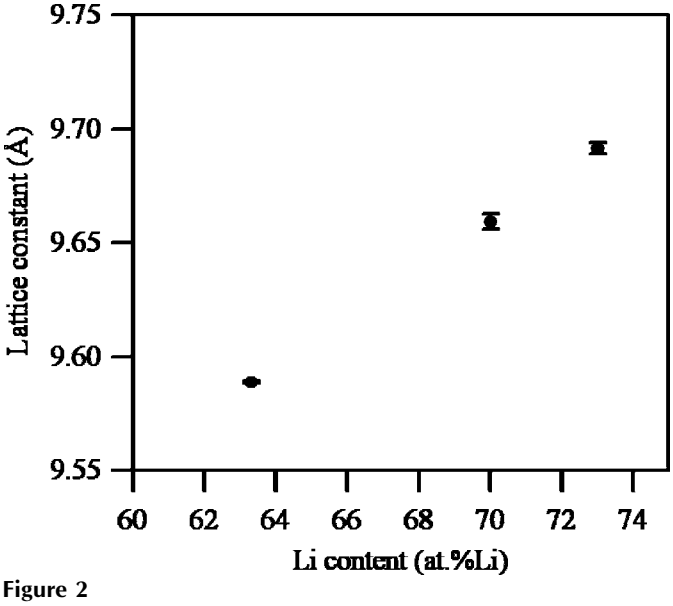

Figure 2
Li concentration dependence of the lattice constant for the Ag–Li gamma-brass. Note that the least Li-bearing sample was employed for crystal structure determination, in which the Li concentration of the gamma-brass phase was fixed to be 64.3 at.%. This is slightly different from the nominal concentration of 63.3 at.% employed here.

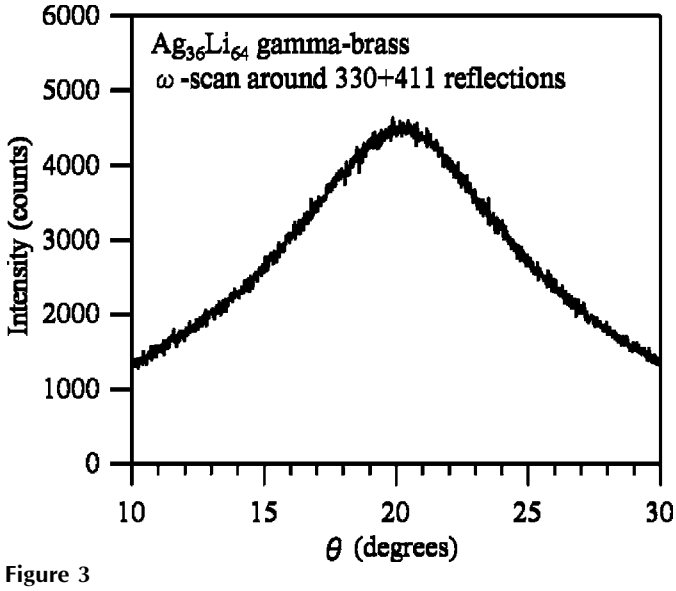

Figure 3
ω-scan profile around the 330 + 411 diffraction peak for the $Ag_{36}Li_{64}$ powdered sample.

3. Results

The crystal structure was refined by assuming that the γ-phase coexists with the residual β-phase and the minute third phase. The diffraction pattern obtained for the refined structure is shown along with the measured one in Fig. 4, in which the difference pattern is also plotted. As listed in the inset to Fig. 4, the reliability factors R_{wp}, R_R, R_I and S are reduced to satisfactory levels.

The third phase was attributed to lithium silver oxide, since its strongest peak appearing at 8.03° in Fig. 4 increased when the ordinary X-ray diffraction measurement with Cu $K\alpha$ radiation was repeated several hours later for the sample in a less accurately isolated condition against exposure to air. The sample measured at SPring-8 was encapsulated into a capillary tube and remained fully intact against oxidation. Regarding the third phase, the lattice constants [a = 3.9823 (6), c = 8.292 (2) Å] and space group ($I4_1/amd$) were found to best reproduce the measured peaks, which were, however, not intense enough to determine the atom positions and chemical composition of Ag–Li–O. $Ag_2Li_0O_1$ was assumed in the final refinement. As mentioned earlier, the present sample was annealed at 458 K for 10 d. According to the phase diagram (Okamoto, 2000), the present sample could be assumed in the two-phase region at 458 K and separated into the γ phase with its limiting composition of $Ag_{35.7}Li_{64.3}$ and the β phase with that of $Ag_{41.1}Li_{58.9}$. In other words, the structure of both γ and

[1] Supplementary data for this paper are available from the IUCr electronic archives (Reference: AV5091). Services for accessing these data are described at the back of the journal.

Table 1
Experimental details.

Crystal data	
Chemical formula	$Ag_{18.56}Li_{33.44}$
M_r	2234.14
Cell setting, space group	Cubic, $I\bar{4}3m$
Temperature (K)	300
a, b, c (Å)	9.6066 (8), 9.6066 (8), 9.6066 (8)
V (Å^3)	886.56 (13)
Z	1
D_x (Mg m^{-3})	4.185
Radiation type	Synchrotron
μ (mm^{-1})	3.85
Specimen form, color	Cylinder, grey
Specimen size	0.2 mm diameter, 3.0 mm length
Specimen preparation cooling rate (K min^{-1})	Unknown (furnace cooling)
Specimen preparation pressure (kPa)	100
Specimen preparation temperature (K)	Melting: *ca* 927; heat treatment: 458
Data collection	
Diffractometer	BL02B2
Data collection method	Specimen mounting: powder inserted in glass capilary in Ar atmosphere; fine powders encapsulated into a capillary glass tube with the diameter of 0.2 mm in the glovebox and sealed the tube with resin to protect the sample from oxidation; mode: transmission; scan method: no scanning [using the steady two-dimensional detector (IP)]
Absorption correction	None
2θ (°)	$2\theta_{min}$ = 2.0, $2\theta_{max}$ = 51.99, increment = 0.01
Refinement	
Refinement on	Least-squares refinement by Marquardt method
R factors and goodness-of-fit	R_p = 0.023, R_{wp} = 0.032, R_{exp} = 0.019, R_B = 0.012, S = 1.67
Wavelength of incident radiation (Å)	0.50226
Excluded region(s)	None
Profile function	Pseudo-Voigt
No. of parameters	52
H-atom treatment	No H atoms present
Weighting scheme	$w_i = 1/y_i$; y_i: measured intensities
$(\Delta/\sigma)_{max}$	< 0.0001

Computer programs: *RIETAN*2000 (Izumi & Ikeda, 2000), *ATOMS* (Dowty, 1999).

β phases was refined while fixing their compositions to these limiting values and assuming the absence of vacancy, *i.e.* maintenance of 52 atoms in the unit cell. At the final stage of refinement of the γ-phase, occupancies of the Li atom on IT and CO sites are set equal to unity, while that of the Ag atom on the OH site is further refined under the condition that the total composition is kept at $Ag_{35.7}Li_{64.3}$. The mole fraction of the γ and β phase, and the oxide turned out to be 93.0, 6.9 and 0.1 mol %, respectively. The overall composition $Ag_{36.2}Li_{63.7}O_{0.1}$ after the structure refinement was found to be in good agreement with the nominal one $Ag_{36.7}Li_{63.3}$. Hence, we hereafter refer to the present sample as the $Ag_{36}Li_{64}$ gamma-brass.

Numerical data on the crystal structure for both the γ and β brasses deduced from the Rietveld structure analysis are listed in Table 2. The space group for the γ phase is confirmed to be $I\bar{4}3m$, in contrast to the suspected $P\bar{4}3m$ listed in Okamoto (2000). As already described in §1, the 26-atom cluster is composed of 4, 4, 6 and 12 atoms at vertices of the IT, OT, OH and CO sites, respectively, and is arranged to form the b.c.c. lattice. We conclude that atomic sites on both IT and CO sites are occupied by the Li atom having a larger atomic size, while those on OT and OH sites are occupied by smaller Ag atoms with small amounts of Li atoms existing as chemical disorder. The occupancy of the Ag1 site in the β phase is reduced to 0.822 in conformity with the boundary condition imposed on the Li concentration, *i.e.* $Ag_{41.1}Li_{58.9}$.

4. Discussion

The crystal structure of the gamma-brass can be viewed as stacking b.c.c. lattices three times along x, y and z directions with the subsequent removal of the corner and center atoms from the resulting large cell (Bradley & Thewlis, 1926). The remaining 52 atoms are reshuffled to find the most stable position to release the strain caused by the generation of the two vacancies. It is, therefore, interesting to pursue how atoms on the respective clusters are displaced relative to the position of the original b.c.c. lattice site. We added to Fig. 1 the resulting atom positions on the respective clusters in the $Ag_{36}Li_{64}$ gamma-brass relative to the corresponding polyhedra in the original b.c.c. lattice. A sizeable shrinkage is found to occur in both IT and CO sites, where Li atoms exclusively reside, while a small expansion occurs in both OT and OH sites, where Ag atoms are dominant.

A volume change of each polyhedron upon the formation of the gamma-brass from the b.c.c. lattice is calculated not only for the present $Ag_{36}Li_{64}$ gamma-brass, but also for the Cu_5Zn_8 (Heidenstam *et al.*, 1968; Brandon *et al.*, 1974) and Al_8V_5 gamma-brasses (Brandon, Pearson *et al.*, 1977).[2] As listed in Table 3, the deformation rate defined as $(V_g - V_0)/V_0$, where V_g is the volume of the polyhedron in the gamma-brass and V_0 is the corresponding one in the b.c.c. lattice, is extremely large and negative in sign for the IT polyhedron and exceeds 65% for all three gamma-brasses studied. This obviously occurs to reduce the dead volume at the center of the unit cell. To counterbalance a large shrinkage of the IT polyhedron, volumes of both OT and OH polyhedra are expanded. It is interesting to note that the expansion rate of the OH polyhedron is always approximately 20%, while that of the OT polyhedron is *ca* 10% for all three gamma-brasses studied. The outermost cluster CO polyhedron is again shrunk with its magnitude comparable to that in the OH polyhedron. As

[2] The crystal structure for the Cu_5Zn_8 gamma-brass was experimentally deduced to be perfectly ordered without chemical disorder at any site on IT, OT, OH and CO sites. Instead, the crystal structure of the Al_8V_5 gamma-brass, although existing as a line compound in the phase diagram (Okamoto, 2000), was found to involve chemical disorder in IT and OH sites (see Table 3). The Ag–Li gamma-brass has a wide solid-solution range in its phase diagram (Okamoto, 2000). The present structure analysis for the Ag–Li gamma-brass revealed a composition slightly different from the stoichiometric ratio Ag:Li = 5:8, and involved chemical disorder. Hence, we intentionally refer to the present gamma-brass as $Ag_{36}Li_{64}$, while the other two are Cu_5Zn_8 and Al_8V_5.

Table 2
Crystal structure of $Ag_{36}Li_{64}$ gamma-brass and $Ag_{41}Li_{59}$ beta-brass.

	Site	g	x	y	z	B_{eq}
$Ag_{35.7}Li_{64.3}$ $I\bar{4}3m$ (No. 217) a = 9.6066 (8) Å						
Ag1	OT 8(*c*)	0.931	0.8277 (1)	0.8277	0.8277	1.41
Li1	OT 8(*c*)	0.069	0.8277	0.8277	0.8277	1.41
Ag2	OH 12(*e*)	0.926 (1)	0.3541 (1)	0.0	0.0	1.46
Li2	OH 12(*e*)	0.074	0.3541	0.0	0.0	1.46
Li3	IT 8(*c*)	1.0	0.117 (1)	0.117	0.117	3.33
Li4	CO 24(*g*)	1.0	0.315 (1)	0.315	0.033 (2)	3.08

Interatomic distance (Å)

(*a*) Ag2—Li4 = 2.74 (2)	(*j*) Li3—Li4 = 2.810 (2)	(*i*) Ag1—Ag2 = 2.921 (1)
(*b*) Ag1—Li4 = 2.77 (2)	(*d*) Ag1—Li4 = 2.83 (2)	(*f*) Ag2—Li4 = 3.05 (2)
(*c*) Ag2—Li3 = 2.778 (1)	(*k*) Li4—Li4 = 2.843 (5)	(*g*) Ag2—Li4 = 3.07 (1)
(*h*) Ag2—Ag2 = 2.802 (2)	(*e*) Ag1—Li3 = 2.878 (7)	(*l*) Li3—Li3 = 3.17 (3)

	Site	g	x	y	z	B_{iso}
$Ag_{41.1}Li_{58.9}$ $Pm\bar{3}m$ (No. 221) a = 3.1818 (3) Å						
Ag1	1(*a*)	0.822	0.0	0.0	0.0	1.83 (5)
Li1	1(*a*)	0.178	0.0	0.0	0.0	1.83
Li2	1(*b*)	1.0	0.5	0.5	0.5	1.83

Interatomic distance (Å)
Ag1—Li2 = 2.756 (1)

listed in Table 3, it happens that the larger atoms Li, Zn and Al are filled into CO and IT sites, while the smaller atoms Ag, Cu and V into OT and OH sites.

From the point of view of geometrical considerations, in particular the packing fraction of atoms, it may be natural to locate the larger atoms on the IT polyhedron surrounding the dead volume and smaller atoms on the OT sites surrounding the IT polyhedron. The structure data of the gamma-brass possessing the space group $I\bar{4}3m$ are available in the literature in nine alloy systems (Marsh, 1954; Johansson *et al.*, 1968; Arnberg & Westman, 1972*b*; Edström & Westman, 1969). The atom species entering into the IT and OT sites are listed in Table 4, along with the size ratio of the atom on the IT site over that on the OT site. It turns out that although the size ratio is certainly higher than unity for the $Ag_{36}Li_{64}$, Cu_5Zn_8 and Al_8V_5 gamma-brasses discussed above, the ratio for the Ag_5Zn_8, for example, is definitely lower than unity (Marsh, 1954). Moreover, Cu_5Cd_8 has been known to possess a large size difference between Cu and Cd. Here both IT and OT sites are only occupied by smaller Cu atoms (Bradley & Gregory, 1931; Heidenstam *et al.*, 1968; Brandon *et al.*, 1974). All these facts strongly indicate that occupation by the larger atom on IT sites and by the smaller atom on OT sites is not crucial in deciding the gamma-brass structure.

In order to gain further insight into the atom distribution over clusters, we have calculated the radial distribution (RD) function of atoms from the refined structure for the present $Ag_{36}Li_{64}$ along with both Cu_5Zn_8 (Brandon *et al.*, 1974) and Al_8V_5 (Brandon, Pearson *et al.*, 1977). The results are plotted in Fig. 5 as a function of the radial distance r/a normalized with respect to the respective lattice constants a. The RD function for the original b.c.c. lattice is shown as a reference. Obviously, the two peaks in the b.c.c. lattice represent the coordination numbers eight and six for its nearest and second nearest-neighbor atoms. We see from Fig. 5 that, upon the relaxation into the gamma-brass structure, the two peaks are decomposed into 12 peaks in the region below r/a = 0.34. More important is the fact that the RD function for the $Ag_{36}Li_{64}$ gamma-brass resembles that for the Cu_5Zn_8, but differs in a characteristic manner from that for the Al_8V_5 gamma-brass.

First, we direct our attention to the position of the atomic pair on the IT polyhedron marked as (l) in Fig. 5. The distance, though normalized with respect to the lattice constant a, is the largest in $Ag_{36}Li_{64}$ and then decreases in the order Cu_5Zn_8 then Al_8V_5. According to the structure analysis on Al_8V_5 (Brandon, Pearson *et al.*, 1977), sites on the IT polyhedron are equally shared by Al and V atoms, allowing the largest shrinkage in the distance (l) and, hence, the volume, as listed in Table 3. Indeed, an average value of the metallic radii for Al and V atoms is slightly smaller than that of Zn. The volume shrinkage is the smallest in Ag_5Li_8 as a result of the fact that the largest atom Li exclusively occupies sites on the IT polyhedron. Therefore, the difference in the bonding length in (l) in the three systems is essentially understood as the size effect. The discussion so far is apparently consistent with the hard-sphere model developed by Brandon, Brizard, Pearson &

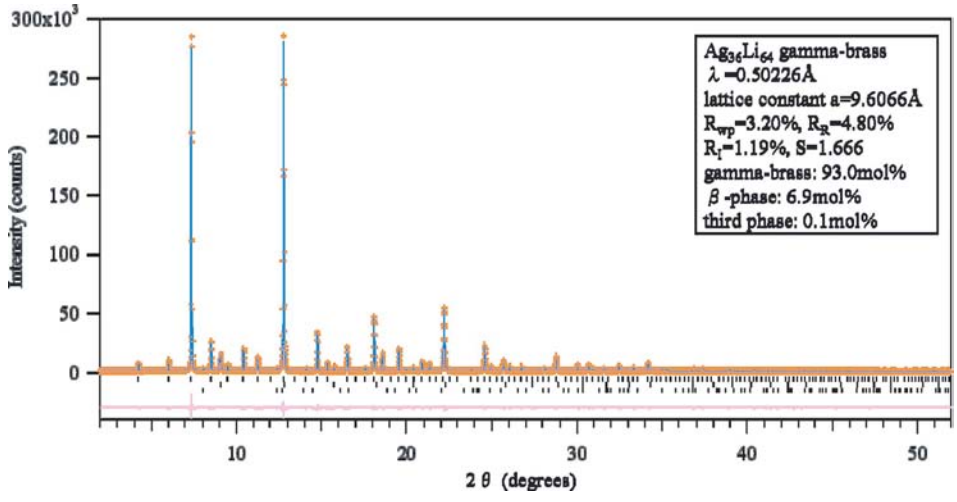

Figure 4
Rietveld structure analysis for the $Ag_{36}Li_{64}$ powdered sample. +: measured data; solid line: calculated data. The difference between observed and calculated intensities is plotted underneath. The resulting reliability factors are listed in the inset.

Table 3
Volume of the four polyhedra in the 26-atom cluster in the three gamma-brasses.

Alloys	$Ag_{36}Li_{64}$				Cu_5Zn_8				Al_8V_5			
Size ratio r_{IT}/r_{OT}	1.081				1.091				1.032			
Clusters	IT	OT	OH	CO	IT	OT	OH	CO	IT	OT	OH	CO
V_g (Å^3)	3.768	12.10	52.50	68.94	2.452	9.374	41.21	52.00	2.515	10.32	45.86	55.73
V_0 (Å^3)	10.95	10.95	43.78	87.56	8.528	8.528	34.11	68.23	9.623	9.720	38.88	77.76
$\Delta V/V_0$	−65.6	10.5	19.9	−21.3	−71.3	9.9	20.8	−23.8	−74.1	6.1	18.0	−28.3
Dominant atoms	Li	Ag	Ag	Li	Zn	Cu	Cu	Zn	Al/V	V	V	Al
Metallic radius (Å)	1.562	1.445	1.445	1.562	1.394	1.278	1.278	1.394	1.389†	1.346	1.346	1.432

† In the case of Al_8V_5, the IT sites are occupied by Al and V atoms with equal probabilities. Hence, an atomic radius of 1.389 Å was assigned by taking an average of the metallic radii of Al (1.432 Å) and V (1.346 Å).

Tozer (1977) to discuss the structure of gamma-brasses with the space groups of both $I\bar{4}3m$ and $P\bar{4}3m$. However, a closer inspection into the RD functions for the $Ag_{36}Li_{64}$, Cu_5Zn_8 and Al_8V_5 gamma-brasses in Fig. 5 reveals a distinctive difference in the distribution of pairs of atoms on OH and CO sites. A pair connecting an atom on the OH polyhedron with that on the CO polyhedron involves three different bonds: a, f and g. As illustrated in Figs. 6(*a*) and (*b*), the bonds a and f refer to the pairs connecting the atom on the OH polyhedron in the cluster with that on the CO polyhedron in the neighboring clusters, whereas bond g refers to the pair within the cluster. The bond lengths of f and g are found to be close to each other, but are separated from the shortest one in a in Cu_5Zn_8 and $Ag_{36}Li_{64}$. In contrast, bond lengths of f and g are more widely separated in Al_8V_5. Indeed, the difference defined as $\Delta_{f-g} \equiv 2\{(r/a)_f - (r/a)_g\}/\{(r/a)_f + (r/a)_g\}$ turned out to be −0.69, +0.81 and +4.6% for $Ag_{36}Li_{64}$, Cu_5Zn_8 and Al_8V_5, respectively, the last one being almost six times as large as the first two.

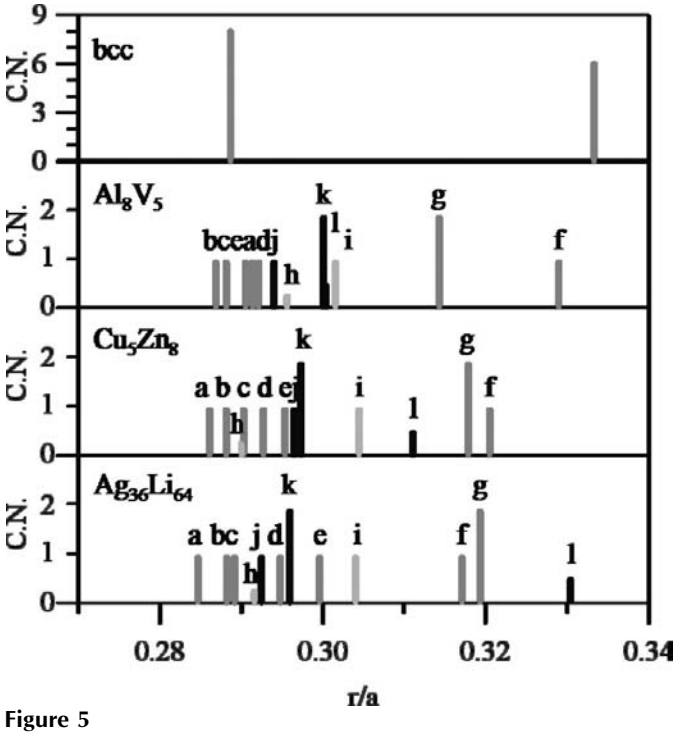

Figure 5
Radial distribution functions of atoms calculated for the three gamma-brasses $Ag_{36}Li_{64}$, Cu_5Zn_8 (Brandon *et al.*, 1974) and Al_8V_5 (Brandon, Pearson *et al.*, 1977) relative to that for the b.c.c. lattice. The abscissa represents the atomic pair distance normalized with respect to the respective lattice constants, whereas the ordinate represents the coordination number. In the case of the b.c.c. structure having the lattice constant *a* of the gamma-brass, the nearest and second nearest neighbors possessing the coordination numbers 8 and 6 are located at the positions of $r/a = (3)^{1/2}/6 = 0.288$ and $r/a = a/3 = 0.333$, respectively. Atom pairs are specified by letters a to l (see Table 1 for the definition).

It is interesting to examine why bond lengths of f and g are similar to each other in Cu_5Zn_8 and $Ag_{36}Li_{64}$, while they are well separated in Al_8V_5. First, we checked the bond angle of the a, f and g pairs, which is defined as shown in Fig. 6(*c*), relative to the *z* axis connecting atoms on the top and bottom vertices of the OH polyhedron, and is calculated for the three gamma-brasses. As listed in Table 5, the departure of the bond angle from that in the b.c.c. lattice is the smallest for f, but the largest for a. As far as the bond angle is concerned, there is no substantial difference among the three gamma-brasses. Fig. 7 shows a comparison of the geometrical configuration for the three bonds a, f and g between the $Ag_{36}Li_{64}$ and Al_8V_5 gamma-brasses. To allow a direct comparison in magnitude, both bonds f and g are drawn so as to fall in the plane of the paper. Unfortunately, however, $\Delta_{f-g} = +4.6\%$ for Al_8V_5 is still too small to differentiate between the two bonds f and g, even in the magnified view in Fig. 7.

The RD function of the Ag_5Zn_8 gamma-brass is also calculated from the structure data (Marsh, 1954). The same characteristic feature as that in the Cu_5Zn_8 and Ag_5Li_8 is found regarding the position of the atomic pairs a, f and g, although it is different from them in the sense that the smaller atom Zn enters into the CO polyhedron and the larger atom Ag into the OH polyhedron. As a matter of fact, the value of Δ_{f-g} is merely +0.40%, being comparable to those in Cu_5Zn_8 and Ag_5Li_8, but smaller by one order of magnitude than that in Al_8V_5.

Judging from the arguments above, we believe the +4.6% difference in the bond length of f and g in the Al_8V_5 to originate from its electronic structure. The first-principles FLAPW band calculations have already been performed for the Cu_5Zn_8 (Asahi *et al.*, 2005*a*,*b*) and Al_8V_5 gamma-brasses (Mizutani *et al.*, 2006). The resonance of mobile electrons near the Fermi level with the set of {411} and {330} lattice planes is proved to play a key role in the formation of the pseudogap in the Cu_5Zn_8 gamma-brass. In the case of the Al_8V_5 gamma-brass, an experimentally derived crystal structure (Brandon,

Pearson *et al.*, 1977) was simplified such that the IT sites were fully replaced by Al atoms, whereas those on the OH site were replaced by V atoms, since the ordered structure was needed for the band calculations (Mizutani *et al.*, 2006). It turned out that orbital hybridization, particularly between the V-3*d* states on the OH polyhedron and Al-3*p* states on the CO polyhedron, is largely responsible for the splitting of the V-3*d* band into bonding and antibonding states, resulting in a deep pseudogap at 0.5 eV above the Fermi level (Mizutani *et al.*, 2006). The *d*–*p* hybridization discussed above is definitely weak in the Cu_5Zn_8 and Ag_5Zn_8 gamma-brasses, since the Cu and Ag *d* bands are immersed well below the Fermi level (Asahi *et al.*, 2005*a*,*b*; Mizutani *et al.*, 2004). Thus, we consider the difference in the degree of the *d*–*p* hybridization to be reflected in atomic arrangements on CO and OH sites between Cu_5Zn_8 and Al_8V_5 gamma-brasses.

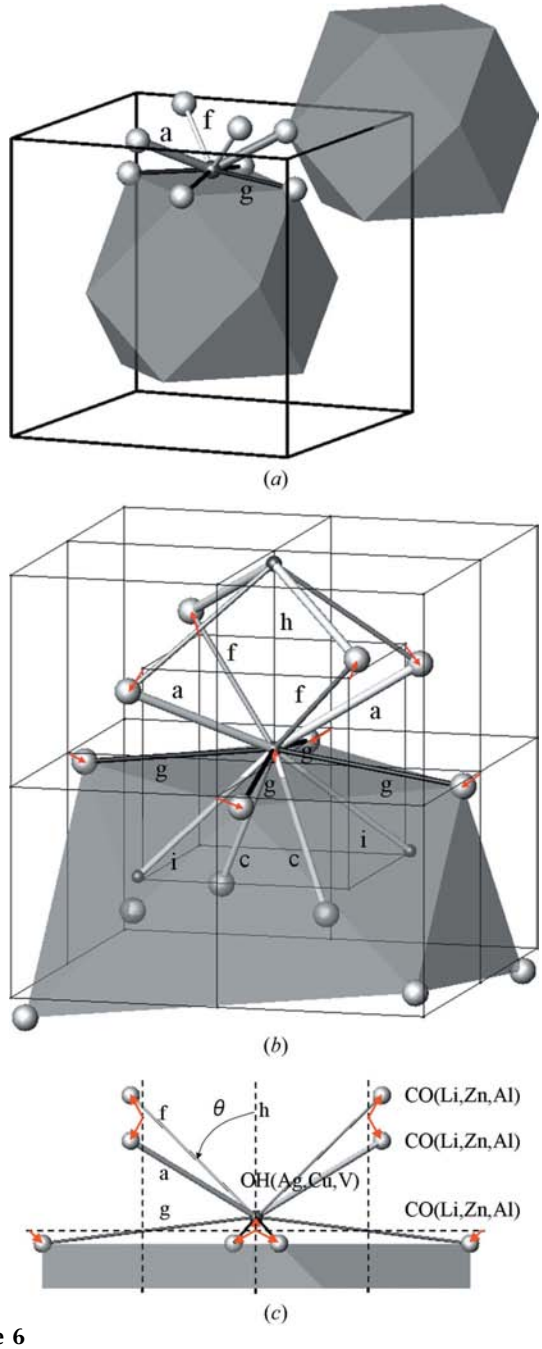

Figure 6
(*a*) Atomic pairs a, f and g on the two 26-atom clusters in the unit cell of the gamma-brass, (*b*) atoms on CO, IT and OH sites and relevant atomic pairs in the central 26-atom cluster. The cage indicates the original b.c.c. lattice and a small arrow the displacement vector of an atom relative to the b.c.c. lattice, (*c*) its cross-sectional view to define the bond angle θ for the atomic pairs a, f and g for the three gamma-brasses. The displacement vector relative to the b.c.c. lattice is also shown.

Table 4
Size ratio of atoms on IT over those on OT in different gamma-brasses with the space group $I\bar{4}3m$.

	Majority atom on IT	Majority atom on OT	r_{IT}/r_{OT}
$Ag_{36}Li_{64}$ [(a)]	Li	Ag	1.081
Ag_5Zn_8 [(b)]	Zn	Ag	0.965
Al_8V_5 [(c)]	Al/V	V	1.032
Cu_5Cd_8 [(d, e, f)]	Cu	Cu	1.000
Cu_5Zn_8 [(e, f)]	Zn	Cu	1.091
$Co_{20}Zn_{80}$ [(g)]	Zn	Co	1.113
Fe_3Zn_{10} [(f, h)]	Zn	Fe	1.094
Ir_2Zn_{11} [(i)]	Zn	Ir	1.027
$Ni_{20}Zn_{80}$ [(h)]	Zn	Ni	1.119
Pd_6Zn_{20} [(j)]	Zn	Pd	1.013

References: (*a*) present work; (*b*) Marsh (1954); (*c*) Brandon, Pearson *et al.* (1977); (*d*) Bradley & Gregory (1931); (*e*) Heidenstam *et al.* (1968); (*f*) Brandon *et al.* (1974); (*g*) Asahi *et al.* (2005*b*); (*h*) Johansson *et al.* (1968); (*i*) Arnberg & Westman (1972*a*,*b*); (*j*) Edström & Westman (1969).

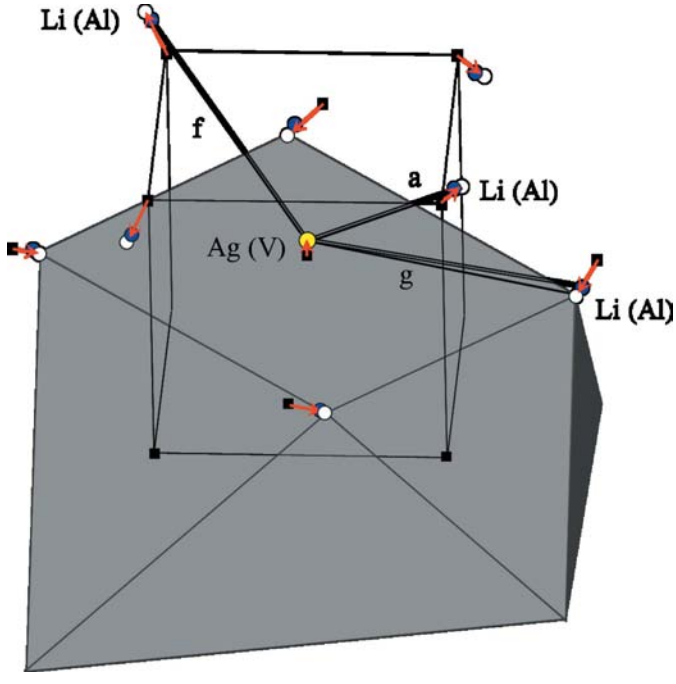

Figure 7
The three bonds a, f and g obtained by connecting the atom on the OH polyhedron with that on the CO polyhedron. Part of the 26-atom cluster is shown by the polyhedron. Open and solid circles indicate Li and Al atoms on the CO polyhedron in the $Ag_{36}Li_{64}$ and Al_8V_5 gamma-brasses, respectively. The atom immediately above the center of the square face of the polyhedron corresponds to the OH site and refers to either the Ag or V atom. A small solid square and an arrow indicate the lattice site in the b.c.c. lattice and displacement vector, respectively. Both bonds f and g are in the plane of the paper.

Table 5
Bond angle of pairs connecting atoms on OH and CO relative to the z axis in the three gamma-brasses.

	b.c.c.	$Ag_{36}Li_{64}$			Cu_5Zn_8			Al_8V_5		
	θ	Atom on CO	θ	$\Delta\theta$	Atom on CO	θ	$\Delta\theta$	Atom on CO	θ	$\Delta\theta$
a	54.7	Li	66.7	12.0	Zn	67.6	12.9	Al	68.2	13.4
f	54.7	Li	55.6	0.8	Zn	55.6	0.9	Al	55.3	0.6
g	90.0	Li	97.0	7.0	Zn	97.6	7.6	Al	98.0	8.0

The atoms on the OH are Ag, Cu and V in the respective gamma-brasses. $\Delta\theta$ indicates the departure of the bond angle from that in the b.c.c. lattice.

A similarity in the RD function of $Ag_{36}Li_{64}$ to that of Cu_5Zn_8 suggests the resemblance of the electronic structure between them. At this stage, we comment on the solid solubility range of the gamma-brass. Both the Cu_5Zn_8 and Ag_5Zn_8 gamma-brasses possess the *d* band due to the noble metal constituent element well below the Fermi level and, hence, are characterized by rather weak *d–p* hybridization near the Fermi level. This most likely holds true for the present $Ag_{36}Li_{64}$. The nearly free-electron-like electronic structure would allow a more isotropic distribution of atoms. This may explain why all these gamma-brasses possess a finite solid solution range. In contrast, the *d* states owing to V in the Al_8V_5 gamma-brass are spread widely across the Fermi level. Thus, they are characterized by strong *d–p* orbital hybridization (Mizutani *et al.*, 2006). Now more directional bonding must be developed. This would explain why the bond lengths in f and g are split by more than 4.5% in Al_8V_5, and are responsible for its existence as a line compound in the phase diagram (Okamoto, 2000). A similar situation is expected to occur in the Mn_3In gamma-brass also existing as a line compound (Okamoto, 2000).

Finally, it may be worthwhile noting that the present structure determination was made to allow the first-principles electronic structure calculations for the $Ag_{36}Li_{64}$ gamma-bass, since it is obviously at variance with the Hume–Rothery electron concentration rule demanding its stability at e/a = 21/13. The determination of the crystal structure in the present work is of vital importance. As listed in Table 2, the experimentally derived structure involves slight chemical disorder only in OT and OH sites. An ordered structure may be constructed by ignoring the minor element of Li on OT and OH sites. The crystal structure is then simplified such that IT, OH, OT and CO sites are exclusively occupied by 4 Ag, 6 Ag, 4 Li and 12 Li atoms in the 26-atom cluster, respectively, leading to the composition Ag_5Li_8 with the space group $I\bar{4}3m$. The first-principles band calculations for the Ag_5Li_8 gamma-brass are in progress.

5. Conclusions

We revealed that the $Ag_{36}Li_{64}$ gamma-brass contains 52 atoms in its unit cell with the space group $I\bar{4}3m$ and that the occupancy of the Li atom at the IT and CO sites is 100%, whereas that of the Ag atom at the OT and OH sites is more than 90%, indicating the presence of small chemical disorder on both OT and OH sites. The crystal structure thus deduced was compared with those already available in the literature, particularly that of Cu_5Zn_8 and Al_8V_5. The bond lengths between the transition metal atom on the OH site and the non-transition metal atom on CO sites were found to reflect the degree of orbital hybridization between these two elements. Judging from its behavior, we suggested that the orbital hybridization effect would be weak in the $Ag_{36}Li_{64}$ gamma-brass and that its electronic structure near the Fermi level would be well described in terms of the nearly free-electron model.

One of the authors (UM) is grateful to Professor H. Sato, Aichi University of Education, for valuable discussions on the role of orbital hybridization in the Al_8V_5 gamma-brass. UM also thanks the Japan Society for the Promotion of Science for financial support from a Grant-in-Aid for Scientific Research (Contract No. 17560583). The synchrotron radiation experiments were performed at the BL02B2 in the SPring-8 with the approval of the Japan Synchrotron Radiation Research Institute (JASRI; Proposal No. 2006B1039).

References

Arnberg, L. & Westman, S. (1972*a*). *Acta Chem. Scand.* **26**, 1748–1750.
Arnberg, L. & Westman, S. (1972*b*). *Acta Chem. Scand.* **26**, 513–517.
Asahi, R., Sato, H., Takeuchi, T. & Mizutani, U. (2005*a*). *Phys. Rev. B*, **71**, 165103.
Asahi, R., Sato, H., Takeuchi, T. & Mizutani, U. (2005*b*). *Phys. Rev. B*, **72**, 125102.
Bradley, A. J. (1929). *Philos. Mag.* **6**, 878–888.
Bradley, A. J. & Gregory, C. H. (1931). *Philos. Mag.* **12**, 143–162.
Bradley, A. J. & Jones, P. (1933). *J. Inst. Met.* **51**, 131–162.
Bradley, A. J. & Thewlis, J. (1926). *Proc. R. Soc. London Ser. A*, **112**, 678–692.
Brandon, J. K., Brizard, R. Y., Chieh, P. C., McMillan, R. K. & Pearson, W. B. (1974). *Acta Cryst.* B**30**, 1412–1417.
Brandon, J. K., Brizard, R. Y., Pearson, W. B. & Tozer, D. J. N. (1977). *Acta Cryst.* B**33**, 527–537.
Brandon, J. K., Pearson, W. B., Riley, P. W., Chieh, C. & Stokhuyzen, R. (1977). *Acta Cryst.* B**33**, 1088–1095.
Dowty, E. (1999). *ATOMS*. Shape Software, 521 Hidden Valley Road, Kingsport, TN 37663, USA.
Ekman, W. (1931). *Z. Phys. Chem. Abt. B*, **12**, 57–78.
Edström, V. A. & Westman, S. (1969). *Acta Chem. Scand.* **23**, 279–285.
Freeth, W. E. & Raynor, G. V. (1953–1954). *J. Inst. Met.* **82**, 569–574.
Heidenstam, O. von, Johansson, A. & Westman, S. (1968). *Acta Chem. Scand.* **22**, 653–661.
Izumi, F. & Ikeda, T. (2000). *Mater. Sci. Forum*, **321–324**, 198–203.
Johansson, A., Ljung, H. & Westman, S. (1968). *Acta Chem. Scand.* **22**, 2743–2753.
Marsh, R. E. (1954). *Acta Cryst.* **7**, 379.
Mizutani, U., Takeuchi, T. & Sato, H. (2004). *Prog. Mater. Sci.* **49**, 227–261.
Mizutani, U., Asahi, R., Sato, H. & Takeuchi, T. (2006). *Phys. Rev. B*, **74**, 235119.
Mott, N. F. & Jones, H. (1936). *The Theory of Properties of Metals and Alloys.* Oxford: Clarendon Press.

Okamoto, H. (2000). *Phase Diagrams for Binary Alloys.* Materials Park, Ohio: ASM International.
Pearson, W. B. (1972). *Crystal Chemistry and Physics of Metals and Alloys*, p. 151. New York: Wiley-Interscience.
Pastorello, S. (1930). *Gazz. Chim. Ital.* **60**, 493.
Pastorello, S. (1931). *Gazz. Chim. Ital.* **61**, 47–51.
Perlitz, H. (1933). *Z. Kristallogr.* **86**, 155.
Westgren, A. & Phragmen, G. (1928). *Metallwirtschaft*, **7**, 700–703.
Westgren, A. F. & Phragmen, G. (1929). *Trans. Faraday Soc.* **25**, 379–385.
Witte, H. (1937). *Metallwirtschaft*, **16**, 237–245.